applied nano

MDPI

Article

Design of ZnO-Drug Nanocarriers against the Main Protease of SARS-CoV-2 (COVID-19): An In Silico Assay

Erik Díaz-Cervantes [1], Cristal Zenteno-Zúñiga [1], Vicente Rodríguez-González [2] and Faustino Aguilera-Granja [3,*]

[1] Centro Interdisciplinario del Noreste (CINUG), Departamento de Alimentos, Universidad de Guanajuato, Tierra Blanca, Guanajuato 37975, Mexico; e.diaz@ugto.mx (E.D.-C.); crizenzu9801@gmail.com (C.Z.-Z.)
[2] División de Materiales Avanzados, Instituto Potosino de Investigación Científica y Tecnológica (IPICYT), San Luis Potosí 78216, Mexico; vicente.rdz@ipicyt.edu.mx
[3] Instituto de Física, Universidad Autónoma de San Luis Potosí, San Luis Potosí 78000, Mexico
* Correspondence: faustino@ifisica.uaslp.mx

Abstract: The treatment of coronavirus diseases (COVID-19) is a principal aim worldwide that is required restore public health in the population. To this end, we have been studied several kinds of de novo and repurposed drugs to investigate their ability to inhibit the replication of the virus which causes the current pandemic—the severe acute respiratory syndrome coronavirus 2 (SARS-CoV-2). However, finding a vehicle that promotes the controlled dosage is vital for avoiding secondary effects. For this reason, the present work exposes a nanostructured carrier based on ZnO, which is coupled to three repurposed drugs (Chloroquine, Dipyridamole, and Lopinavir) to understand the chemical interaction of the formed composite. The designed composites are modeled and optimized using the DFT formalism. In obtaining exergonic adsorption energies, we found values between 0.582 to 2.084 eV, depending on the used drug. At the same time, the HOMO orbitals demonstrate the electronic overlap between the ZnO-Np and the Lopinavir, which is the molecule with the higher adsorption energy. Finally, we carried out a docking assay to investigate the interaction of free drugs and composites with the main protease of the SARS-CoV-2, finding that the coupling energy of the composites (at around to 0.03 eV) was higher, compared with the free drugs. As such, our results suggest a controlled dosage of the drug on the SARS-CoV-2 target.

Keywords: ZnO-NPs; nano-carriers; SARS-CoV-2; DFT; molecular-docking

Citation: Díaz-Cervantes, E.; Zenteno-Zúñiga, C.; Rodríguez-González, V.; Aguilera-Granja, F. Design of ZnO-Drug Nanocarriers against the Main Protease of SARS-CoV-2 (COVID-19): An In Silico Assay. *Appl. Nano* **2021**, *2*, 257–266. https://doi.org/10.3390/applnano2030018

Academic Editor: Dimitrios Bikiaris

Received: 30 July 2021
Accepted: 1 September 2021
Published: 3 September 2021

1. Introduction

The current pandemic caused by the coronavirus disease (COVID-19) has affected the world population, causing more than four million deaths and infection in 185 million people worldwide [1]. Considering the psychological and economic damages to society, it is one of the most significant global phenomena in recent decades [2,3]. Today, several sub-types of the virus (alpha to delta) promote COVID-19, the severe acute respiratory syndrome coronavirus 2 (SARS-CoV-2) [4].

Regarding COVID-19, several research groups have been working to find a cure for this disease, considering both a de novo drug design [5,6] and the use of drug repurposing [7–9]. Researchers have considered molecular dynamics, molecular docking, and virtual screening in order to find a novel molecule or an FDA-approved drug that can inhibit SARS-CoV-2 replication. At the same time, the molecular targets to these compounds play a vital role in the drug design, which have been reported mainly as one surface protein of the virus, a so-called spike [10], and as the main protease or 3C-like protease (SARS-CoV-2-M^{Pro}) [11–14]. The last target (yet one of the most commonly-used techniques in drug design), using drug repurposing [15], is the phytochemical compounds [16] which are of a biochemical nature. Nevertheless, our research group has reported one non-protein protease inhibitor [17] which works to inhibit and stop the replication process of this novel virus.

The main complication with some repurposed drugs is the delivery process, which can promote secondary effects. In light of the considerations quoted above, the use of ZnO nanoparticles (ZnO-NPs) has been reported in state-of-the-art nano-compounds [18,19] as a system for drug delivery. In addition, these kinds of systems have been used as a nano-carrier of antibiotics [20]. Furthermore, ZnO-NPs have been studied as antiviral molecules against the H1N1 influenza virus and one of the most widespread viruses—the herpes virus-1 [21,22]. Nevertheless, the electronic interaction of these systems is widely reported, with studies mainly investigating the electronic structure of clusters of ZnO, which have cubic and irregular icosahedral shapes [23]. For these reasons, in the present work we proposed the computational study of two single models of nanoparticles of ZnO interacting with three repurposed drugs—Chloroquine (Clq), dipyridamole (Dip), and lopinavir (Lop)—with the intention of finding the formation of these kinds of composites and their orbital interactions. Once the stable composite was optimized, it was carried out in a docking assay with the SARS-CoV-2-M^{Pro} to evaluate the ligand-target interaction, which can promote the replication of the SARS-CoV-2 virus (COVID-19).

2. Materials and Methods

The nanoparticles of ZnO and the repurposed molecules, Chloroquine, Dipyridamole, and Lopinavir, were modeled using the Avogadro software [24]. The whole molecules were optimized through the Gaussian 09 (G09) package [25], using the formalism of the density functional theory (DFT) at the level of the hybrid functional M06L [26,27], using the basis set 6-31G(d,p) [28] and the pseudopotential LANL2DZ [29] for the Zn atoms. The above level of theory was selected to obtain a complex orbital interaction.

To evaluate the importance of the nanoparticle size, a medium-sized model of the ZnO-NP was designed and optimized with the SIESTA software [30] at PBE [31] level. The above approach was performed due to the lower computing time, derived of the great molecule computed.

$$\text{Drug} + \text{ZnO} - \text{NP} \rightarrow \text{Drug} - \text{ZnO} \quad (1)$$

$$E_{\text{ads}} = E_{\text{composite}} - (E_{\text{ZnO}-\text{NP}} + E_{\text{drug}}) \quad (2)$$

The adsorption energy of the drugs on the ZnO-NP was evaluated using Equations (1) and (2), which evaluated the chemical reaction of adsorption of the drugs. This highlighted that the adsorption energy can be considered as coupling energy. Moreover, the binding energies of the systems (Free drugs, ZnO-NPs and composites) were computed using the Equation (3).

$$E_{\text{b}} = E_{\text{molecule}} - (\sum E_{\text{isolated total atoms}}) \quad (3)$$

Once the models have been optimized and computed, their adsorption energies were carried out in an in silico molecular coupling assay to obtain the interactions between the designed models with the SARS-CoV-2-M^{Pro} (PDB code: 6LU7). The docking assay was performed through the Molegro Virtual Docker package (MVD) [32] through the MolDock scoring function [33].

3. Results

3.1. Binding and Adsorption Energies

The three designed composites, chloroquine coupled to ZnO-NP (ZnO-Clq), Dipyridamole coupled to ZnO-NP (ZnO-Dip), and Lopinavir coupled to ZnO-NP (ZnO-Lop), as well as the ZnO-NP, were optimized with the method described above, obtaining the structures that are depicted in Figure 1.

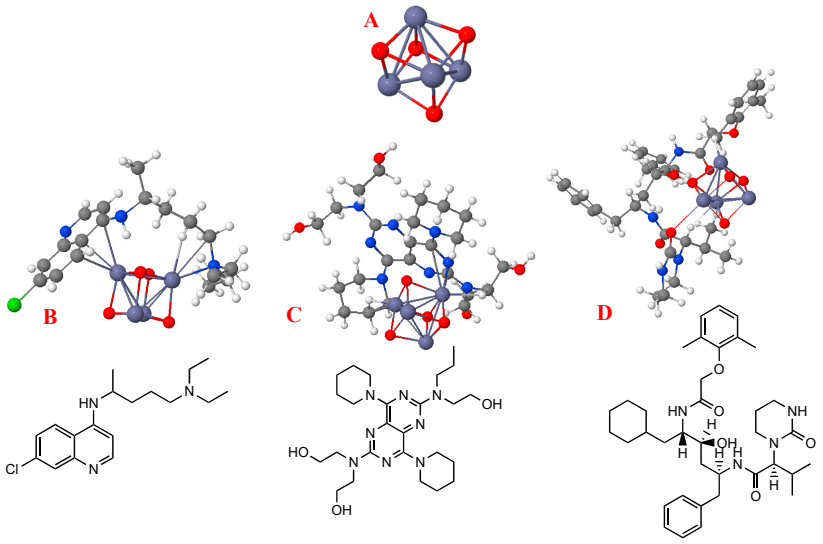

Figure 1. Optimized structures of the (**A**) $(ZnO)_4$-NP model and the three designed composites; (**B**) chloroquine coupled to ZnO-NP ($(ZnO)_4$-Clq); (**C**) Dipyridamole coupled to ZnO-NP ($(ZnO)_4$-Dip), and (**D**) Lopinavir bound to ZnO-NP ($(ZnO)_4$-Lop). Gray spheres represent the carbons, red spheres the oxygens, white spheres the hydrogens, blue spheres are the nitrogens, green spheres represent the chloride, and purple spheres are the zinc atoms.

To evaluate the stabilization of the designed molecules, the binding energies (E_b) were computed, and the results are shown in Table 1. Our results show values of E_b/atom between 4.277 to 4.708.

Table 1. Energy of adsorption, binding energy, and binding energy per atom (in eV), for the studied molecules, using M06L/6-31G(d,p).

Molecule	E_{ads}	E_b	$E_{b/atom}$ *
Clq	-	217.182	4.525
Lop	-	442.528	4.708
Dip	-	337.413	4.440
$(ZnO)_4$	-	20.691	2.586
$(ZnO)_4$-Clq	1.531	239.405	4.275
$(ZnO)_4$-Lop	2.084	465.304	4.562
$(ZnO)_4$-Dip	0.582	358.686	4.270

* E_b/atom = E_b/No. of atoms in the molecule.

In the case of the adsorption energies, Table 1 shows values between 0.582 and 2.084 eV, resulting in the formation of three possible composites, although the $(ZnO)_4$-Lop composite is the more favorable to be synthesized. Note that the binding energy per atom and the adsorption energy match according to the most stable composite.

3.2. Gap Energies and Molecular Orbital Analysis

Table 2 shows the $Gap_{HOMO-LUMO}$ energies for all the molecules here studied, computed at M06L/6-31G(d,p) level. The values oscillate between 2.497 to 4.099 eV. The above indicates that the free drugs present a chemical hardness behavior (with a lower reactivity), which means that the ZnO-NPs make the whole system chemically soften (with a higher reactivity).

Table 2. Gap energies for the studied molecules, in eV.

Molecule	$Gap_{HOMO-LUMO}$
Clq	3.230
Lop	4.099
Dip	2.498
$(ZnO)_4$-NP	2.531
$(ZnO)_4$-Clq	2.638
$(ZnO)_4$-Lop	2.497
$(ZnO)_4$-Dip	2.206

Following the study, the molecular orbitals surfaces were computed and analyzed only in the case of the molecule with the highest adsorption energy. Figures 2A and 3A show the higher interaction of the ZnO-NP, with the electronic density distribution in the whole molecule occurring for the HOMO and LUMO. Furthermore, in Figures 2B and 3B, we show the HOMO-LUMO of the isolated molecule, which demonstrates that the HOMO and LUMO are located on contrasting sites in this molecule. Finally, Figures 2C and 3C show the HOMO and LUMO, respectively, displaying an electronic density distribution between the ZnO-NP and the Lop, and suggesting an adsorption interaction.

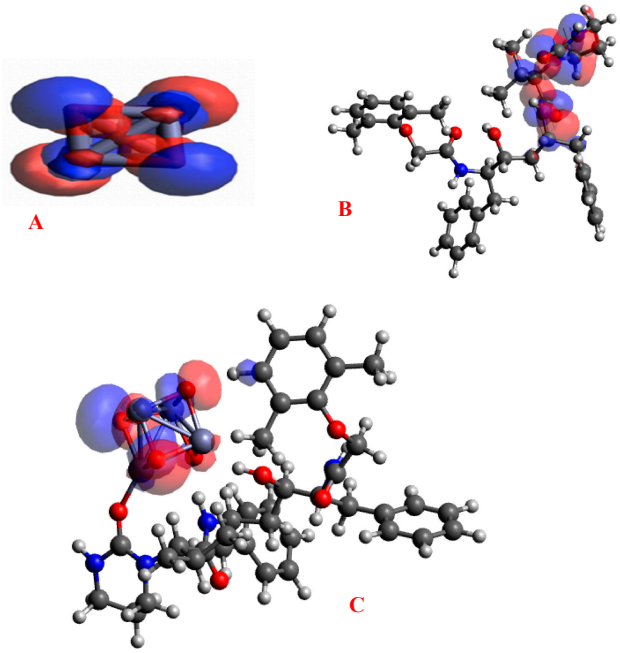

Figure 2. Highest occupied molecular orbitals (HOMO) surfaces for the (**A**) ZnO-NP, (**B**) Lop and (**C**) ZnO-Lop (Isovalue of 0.01).

3.3. Effect of ZnO-NP (Geometric) Structure on Adsorption

Once understanding the adsorption of Clq, Dip, and Lop on the ZnO-NP, was carried out, an analysis of other ZnO-NP was undertaken in order to make a comparison with regard to the effect of the NP size on the adsorption energy of drugs. Figure 4A shows the other designed ZnO-NP, which has 24 atoms ($(ZnO)_{12}$-NP), and considers this in regard to the first ZnO-NP designed and analyzed which at the moment has eight atoms ($(ZnO)_4$-NP), see Figure 1A). Note that, the $ZnO)_{12}$-NP forms an irregular icosahedron, which is partially capped in their triangular faces, forming three bonds.

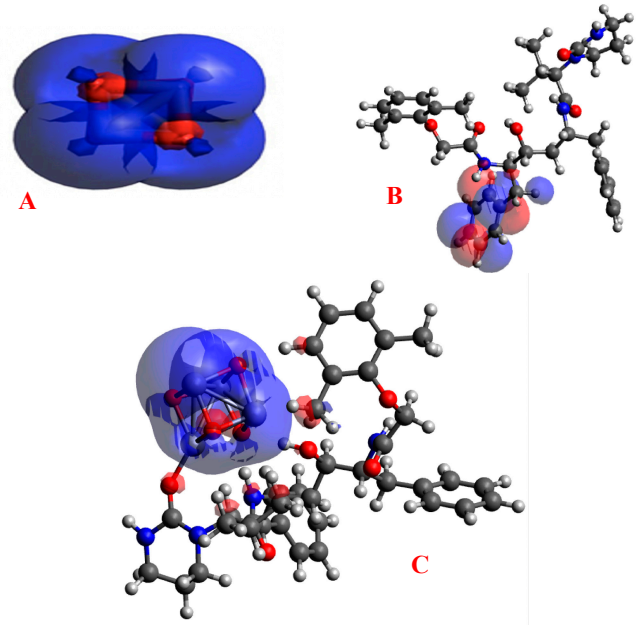

Figure 3. Lowest unoccupied molecular orbitals (LUMO) surfaces for the (**A**) ZnO-NP, (**B**) Lop and (**C**) $(ZnO)_4$-Lop (Isovalue of 0.01).

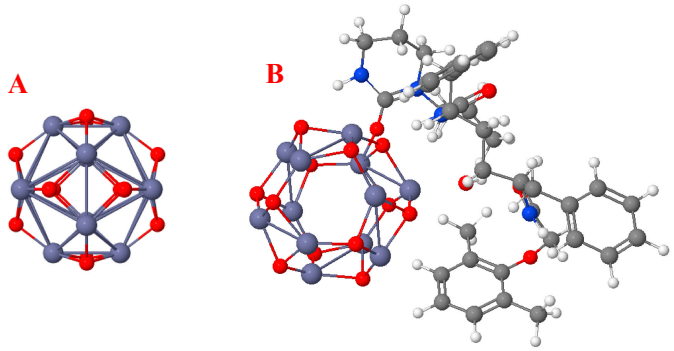

Figure 4. Optimized structures of the (**A**) $(ZnO)_{12}$-NP, and the (**B**) $(ZnO)_{12}$-Lop.

The best-adsorbed drug, Lop, was evaluated and the adsorption of this to the $(ZnO)_4$-NP) and the $(ZnO)_{12}$-NP was computed using the SIESTA package. The results show that the greater NP ($(ZnO)_{12}$-NP) also adsorbs the Lop. This tendency indicates that $(ZnO)_4$-NP) can better adsorb the drug (2.450 eV) than the greater molecule (2.192 eV), due to the surrounding effect of the drug on the small molecule, which results in a size cover by the drug on the NP. It is worth noting that the SIESTA-PBE slightly overestimated the adsorption energy in comparison with G09-M06L, due to the pseudopotential approach.

3.4. Molecular Docking Assay

Finally, the designed composites, the free drugs, and the ZnO-NP were coupled to the SARS-CoV-2-M^{Pro} in order to corroborate the affinity of the studied molecules on this kind of target (which is involved in the replication process of the SARS-CoV-2 virus, causing the current pandemic).

The studied molecules were coupled into the same cavity of the selected target (see Figure 5). The results and the summation of the ligand-target energy are shown in Table 3, which present the values of interaction energy (E) between −2.212 and −8.751 eV and present a ligand efficiency (LE) range from −0.178 to 0.265 eV. Note that the most negative value of LE results in the current molecule being preferred by the target. With regard to this, the best interacting molecule is the ZnO, but the $(ZnO)_4$-Clq is the composite that best interacts with the SARS-CoV-2-MP^{ro}.

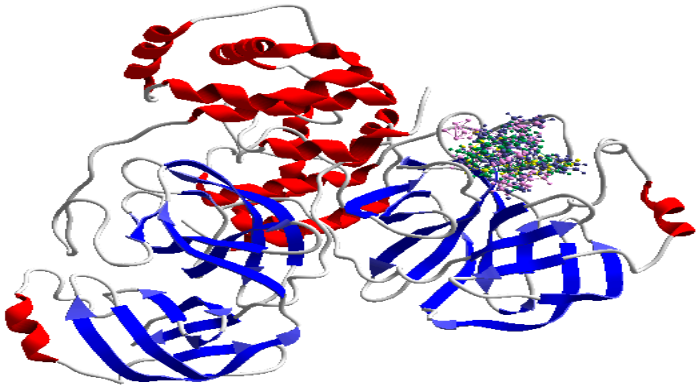

Figure 5. Docking of the studied molecules into the SARS-CoV-2-M^{Pro}.

Table 3. Main interaction energies between the studied molecules and the SARS-CoV-2-M^{Pro}, in eV.

Molecule	E	LE	H-Bond	VdW	Electro
$(ZnO)_4$	−2.121	−0.265	0.000	−0.317	−0.038
Clq	−5.787	−0.263	−0.001	−1.711	0.012
Lop	−8.199	−0.178	−0.182	−1.447	−0.004
Dip	−8.306	−0.231	−0.337	0.866	−0.047
$(ZnO)_4$-Clq	−6.635	−0.221	−0.067	−1.481	0.052
$(ZnO)_4$-Lop	−8.242	−0.153	−0.153	−0.143	0.054
$(ZnO)_4$-Dip	−8.751	−0.199	−0.231	−2.592	0.050
Co-crystal	−9.184	−0.219	−0.363	−2.364	−0.026

E is the whole ligand-target interaction energy; LE is the ligand efficiency = E/No. or heavy atoms; H-bond means the hydrogen bond interactions; VdW is the Van der Waals interactions, and Electro shows the electrostatic interactions.

Furthermore, we analyzed the specific interactions of the best docked free drug (Clq) and the best docked composite ($(ZnO)_4$-Clq) in relation to the selected target (see Figure 6). The ZnO-NP presents electrostatic interactions of repulsion and attraction with His41, see Figure 6A.

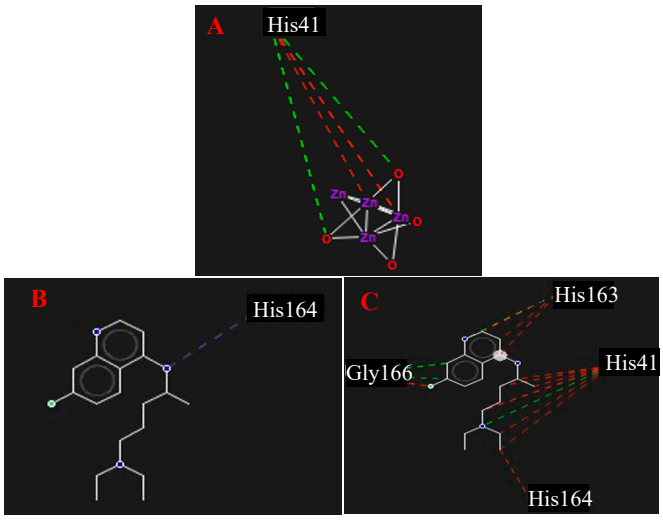

Figure 6. (**A**) Electrostatic interactions between the ZnO-NP with the SARS-CoV-2-MP^{ro}. (**B**) H-bond and (**C**) electrostatic interactions between Clq and the selected target. Green and red lines are the attraction and repulsion electrostatic interactions, respectively, and blue lines depicts the H-bond interactions.

On the other hand, the free Clq shows (Figure 6B,C) H-bond and electrostatic interactions with His164 and only electrostatic repulsion and attraction with His41, His163, and Glu166.

As the better interacting composite, $(ZnO)_4$-Clq presents H-bond interactions with Gly143 (see Figure 7A. At the same time, Figures 6C and 7B show that the same composite presents repulsion interactions with His41 and His163, but the Glu166 promotes an attractive interaction.

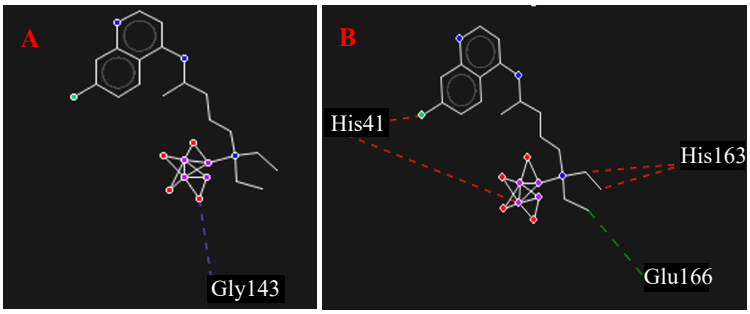

Figure 7. (**A**) H-bond and (**B**) electrostatic interactions between the $(ZnO)_4$-Clq and the SARS-CoV-2-M^{Pro}. Green and red lines are the attraction and repulsion electrostatic interactions, respectively, and blue lines depicts the H-bond interactions.

4. Discussion

4.1. Binding and Adsorption Energies

Figure 1 displays an illustration of the isolated carrier cluster (ZnO-NP) (see Figure 1A), and its interaction between the three selected drugs (see Figure 1B–D.) In ZnO-Clq (Figure 1B), two Zn atoms of the NP are clearly in interaction with carbons and nitrogen of the Clq via hydrogen bonds or directly, which can be promoted by the structural conformation of the NO. In the case of Dip and Lop, the interaction is also between the Zn and the carbon, nitrogen and oxygen of the drugs.

Furthermore, considering the E_b's results, note that the E_b is more comparative if it is calculated per atom. The molecule with the higher internal interaction is lopinavir (with 4.708 eV), due to the higher degrees of freedom promoted by its ramification on the structure. The lower E_b/atom molecule is the ZnO-NP, apparently due to the lower intramolecular interactions and the completely inorganic molecule in Table 1.

When the composites were formed, the binding energy per atom, compared with the free drug, decrease by almost 0.2 eV/atom, but is notably higher than the E_b/atom of the ZnO-NP.

On the other hand, the binding energies demonstrate that in the ZnO-Clq, a composite can be easily formed as well as in the other two drugs, being the least favored in terms of the Dip-composite and the most favored in terms of the Lop-composite. In the case of the Clq, this may be related to the chloride group on the drug, which changes the electronic behavior of the entire system. The other two drugs are N and O, with the promoters of the binding occurring through the Zn.

4.2. Gap Energies and Molecular Orbital Analysis

Concerning the energy gaps, Table 2 clearly shows a decrease in the $E_{HOMO\text{-}LUMO}$ gaps when the composites are formed, due to the weaker isolator character of the ZnO-NP, which results in the compounds tending to narrow their gaps due to the coupling with electrons of the metal oxide NP whose Gap energy is 2.531 eV. Compared with the free molecules, the lopinavir is the system with higher Gap energy, with 4.099 eV, followed by the Clq and the Dip, with values of 3.23 and 2.498 eV, respectively.

Analyzing the molecular orbitals of the best-adsorbed molecule, $(ZnO)_4$-Lop, Figure 2 shows the E_{HOMO} of the free Lop, ZnO-NP, and the composite, which demonstrates the

adsorption interaction of the Lop on the ZnO-NP surface (see Figure 2C) with the electronic density of the higher occupied orbital positioned on both, the ZnO-NP and the Lop.

4.3. Effect of ZnO-NP (Geometric) Structure on Adsorption

The difference of E_{ads} between the $(ZnO)_4$-NP, and the $(ZnO)_{12}$-NP is apparently due to the difference in between both NPs, which can lead to the drug more easily surrounding the small molecule ($(ZnO)_4$-NP), generating an adsorption energy of 2.459 eV, in contrast with the 2.192 eV for the greater molecule ($(ZnO)_{12}$-NP). The level of theory variation was explained in the Results section.

4.4. Molecular Docking Assay

Table 3 shows that the SARS-CoV-2-M^{Pro} prefers to interact with the ZnO-NP than the Clq, despite being considered as a degenerated interaction due to their lower difference (0.002 eV). However, when the ZnO-NP is coupled to the drug, forming the composites, and is evaluated with the selected target, the LE of these systems results is less favorable, decreasing by around 0.03 eV, which can promote a controlled drug delivery.

Analyzing the summation of energies, it is clear that the nanoparticle size is the determinant factor to promote a higher interaction with the SARS-CoV-2-M^{Pro}.

On the other hand, comparing our results with the co-crystallized molecule, the $(ZnO)_4$-Clq composite results better than those mentioned above. However, it is considered degenerated due to its lower difference (0.002 eV).

5. Conclusions

This work was proposed a nanostructured carrier based on ZnO, which was coupled to three repurposed drugs (Chloroquine, Dipyridamole, and Lopinavir) to understand the chemical interaction of the formed composite. The designed composites were modeled and optimized using the DFT formalism, obtaining exergonic adsorption energies (between 0.582 to 2.084 eV), being the better-adsorbed drug the Lop, with an adsorption energy of 2.084 eV. Moreover, E_{HOMO} orbitals demonstrate the electronic overlap between the ZnO-Np and the lopinavir. Finally, we carried out a docking assay in order to observe the interaction of free drugs and composites with the main protease of the SARS-CoV-2, finding that the higher coupling energy of the composites (around to 0.03eV), compared with the free drugs, suggests a controlled dosage of the drug on the SARS-CoV-2-M^{Pro}.

Author Contributions: Conceptualization, E.D.-C. and F.A.-G.; methodology, C.Z.-Z.; validation, E.D.-C. and F.A.-G.; formal analysis, E.D.-C., V.R.-G. and F.A.-G.; investigation, E.D.-C., V.R.-G. and F.A.-G.; resources, E.D.-C. and F.A.-G.; data curation, E.D.-C. and F.A.-G.; writing—original draft preparation, C.Z.-Z.; writing—review and editing, E.D.-C. and F.A.-G.; visualization, E.D.-C., V.R.-G. and F.A.-G.; supervision, F.A.-G. All authors have read and agreed to the published version of the manuscript.

Funding: This research received no external funding.

Institutional Review Board Statement: Not applicable.

Informed Consent Statement: Not applicable.

Acknowledgments: We acknowledge to the Laboratorio Nacional de Caracterización de Propiedades Fisicoquímicas y Estructura Molecular (UG-UAA-CONACYT, Project: 123732) for the computing time provided at the PIPILA cluster.

Conflicts of Interest: The authors declare no conflict of interest.

References

1. World Health Organization. WHO Coronavirus (COVID-19) Dashboard. Available online: https://covid19.who.int/ (accessed on 5 May 2021).
2. Hernigou, J.; Valcarenghi, J.; Safar, A.; Ferchichi, M.A.; Chahidi, E.; Jennart, H.; Hernigou, P. Post-COVID-19 return to elective orthopaedic surgery—is rescheduling just a reboot process? Which timing for tests? Is chest CT scan still useful? Safety of the first hundred elective cases? How to explain the "new normality health organization" to patien. *Int. Orthop.* **2020**, *44*, 1905–1913. [CrossRef]
3. Salameh, P.; Hajj, A.; Badro, D.A.; Acouselwan, C.; Aoun, R.; Sacre, H. Mental Health Outcomes of the COVID-19 Pandemic and a Collapsing Economy: Perspectives from a Developing Country. *Psichiatr. Res.* **2020**, *294*, 113520. [CrossRef] [PubMed]
4. Chen, Y.; Liu, Q.; Guo, D. Emerging coronaviruses: Genome structure, replication, and pathogenesis. *J. Med. Virol.* **2020**, *92*, 418–423. [CrossRef]
5. Cortés-García, C.J.; Chacón-García, L.; Mejía-Benavides, J.E.; Díaz-Cervantes, E. Tackling the SARS-CoV-2 main protease using hybrid derivatives of 1,5-disubstituted tetrazole-1,2,3-triazoles: An in silico assay. *PeerJ* **2020**, *2*, e10. [CrossRef]
6. García-Ramírez, V.; Suarez-Castro, A.; Villa-Lopez, M.; Díaz-Cervantes, E.; Chacón-García, L.; Cortes-García, C. Synthesis of Novel Acylhydrazone-Oxazole Hybrids and Docking Studies of SARS-CoV-2 Main Protease. *Chem. Proc.* **2021**, *3*, 8329. [CrossRef]
7. Parvathaneni, V.; Kulkarni, N.S.; Muth, A.; Gupta, V. Drug repurposing: A promising tool to accelerate the drug discovery process. *Drug Discov. Today* **2019**, *24*, 2076–2085. [CrossRef]
8. Shah, B.; Modi, P.; Sagar, S.R. In silico Studies on Therapeutic Agents for COVID-19: Drug Repurposing Approach. *Life Sci.* **2020**, *252*, 117652. [CrossRef] [PubMed]
9. Kandeel, M.; Al-Nazawi, M. Virtual screening and repurposing of FDA approved drugs against COVID-19 main protease. *Life Sci.* **2020**, *251*, 117627. [CrossRef]
10. Arantes, P.R.; Saha, A.; Palermo, G. Molecular dynamics simulations revealed a promising immune target on the SARS-CoV-2 spike protein, proposing novel strategies for vaccine development. *ACS Cent. Sci.* **2020**, *6*, 1654–1656. [CrossRef]
11. Mpiana, P.T.; Tshibangu, D.S.; Kilembe, J.T.; Gbolo, B.Z.; Mwanangombo, D.T.; Inkoto, C.L.; Lengbiye, E.M.; Mbadiko, C.M.; Matondo, A.; Bongo, G.N.; et al. Identification of potential inhibitors of SARS-CoV-2 main protease from Aloe vera compounds: A molecular docking study. *Chem. Phys. Lett.* **2020**, *754*, 137751. [CrossRef]
12. Zhu, W.; Xu, M.; Chen, C.Z.; Guo, H.; Shen, M.; Hu, X.; Shinn, P.; Klumpp-Thomas, C.; Michael, S.G.; Zheng, W. Identification of SARS-CoV-2 3CL Protease Inhibitors by a Quantitative High-Throughput Screening. *ACS Pharmacol. Trasnl. Sci.* **2020**, *3*, 1008–1016. [CrossRef]
13. Ton, A.-T.; Gentile, F.; Hsing, M.; Ban, F.; Cherkasov, A. Rapid Identification of Potential Inhibitors of SARS-CoV-2 Main Protease by Deep Docking of 1.3 Billion Compounds. *Mol. Inf.* **2020**, *39*, 2000028. [CrossRef]
14. Jin, Z.; Du, X.; Xu, Y.; Deng, Y.; Liu, M.; Zhao, Y.; Zhang, B.; Li, X.; Zhang, L.; Peng, C.; et al. Structure of Mpro from SARS-CoV-2 and discovery of its inhibitors. *Nature* **2020**, *582*, 289–293. [CrossRef] [PubMed]
15. Liu, S.; Zheng, Q.; Wang, Z. Potential covalent drugs targeting the main protease of the SARS-CoV-2 coronavirus. *Bioinformatics* **2020**, *36*, 3295–3298. [CrossRef] [PubMed]
16. Phuong-Thuy, B.T.; Ai-My, T.T.; Thanh-Hai, N.T.; Trung-Hieu, L.; Thai-Hoa, T.; Phuong-Loan, H.T.; Thanh-Triet, N.; Van-Anh, T.T.; Tu-Quy, P.; Van-Tat, P.; et al. Investigation into SARS-CoV-2 Resistance of Compounds in Garlic Essential Oil. *ACS Omega* **2020**, *5*, 8312–8320. [CrossRef] [PubMed]
17. Almaraz-Girón, M.; Calderón-Jaimes, E.; Sánchez-Carrillo, S.; Díaz-Cervantes, E.; Castañón-Alonso, E.; Islas-Jácome, A.; Domínguez-Ortiz, A.; Castañón-Alonso, S. Search for Non-Protein Protease Inhibitors Constituted with an Indole and Acetylene Core. *Molecules* **2021**, *26*, 3817. [CrossRef]
18. Chen, M.; Hu, J.; Bian, C.; Zhu, C.; Chen, C.; Guo, Z.; Zhang, Z.; Agyekum, G.; Zhang, Z.; Cao, X. pH-Responsive and Biodegradable ZnO-Capped Mesoporous Silica Composite Nanoparticles for Drug Delivery. *Materials* **2020**, *13*, 3950. [CrossRef]
19. Babayevska, N.; Iatsunskyi, I.; Florczak, P.; Jarek, M.; Janiszewska, E.; Woźniak, A.; Jurgaa, S. ZnO:Tb3+ hierarchical structures as carriers for drug delivery application. *J. Alloys Compd.* **2020**, *822*, 153623. [CrossRef]
20. Singh, G.; Joyce, E.; Beddow, J.; Mason, T. Evaluation of antibacterial activity of zno nanoparticles coated sonochemically onto textile fabrics. *J. Microbiol. Biotechnol. Food Sci.* **2012**, *2021*, 95–105.
21. Ghaffari, H.; Tavakoli, A.; Moradi, A.; Tabarraei, A.; Bokharaei-Salim, F.; Zahmatkeshan, M.; Farahmand, M.; Javanmard, D.; Kiani, S.; Esghaei, M.; et al. Inhibition of H1N1 influenza virus infection by zinc oxide nanoparticles: Another emerging application of nanomedicine. *J. Biomed. Sci.* **2019**, *26*, 70. [CrossRef]
22. Tavakoli, A.; Ataei-Pirkooh, A.; MM Sadeghi, G.; Bokharaei-Salim, F.; Sahrapour, P.; Kiani, S.; Moghoofei, M.; Farahmand, M.; Javanmard, D.; Monavari, S. Polyethylene glycol-coated zinc oxide nanoparticle: An efficient nanoweapon to fight against herpes simplex virus type 1. *Nanomedicine* **2018**, *13*, 2675–2690. [CrossRef] [PubMed]
23. Cheng, Z.; Li, F.; Zhao, Y. A DFT investigation on ZnO clusters and nanostructures. *J. Mol. Struct.* **2009**, *894*, 121–127. [CrossRef]
24. Hanwell, M.; Curtis, D.; Lonie, D.; Vandermeersch, T.; Zurek, E.; Hutchison, G. Avogadro: An advanced semantic chemical editor, visualization, and analysis platform. *J Cheminformatics* **2012**, *4*, 17. [CrossRef] [PubMed]
25. Frisch, M.J.; Trucks, G.W.; Schlegel, H.B.; Scuseria, G.E.; Robb, M.A.; Cheeseman, J.R.; Scalmani, G.; Barone, V.; Mennucci, B.; Petersson, G.A.; et al. Wallingford CT. 2009. Available online: https://gaussian.com/ (accessed on 31 August 2021).

26. Zhao, Y.; Truhlar, D.G. The M06 suite of density functionals for main group thermochemistry, thermochemical kinetics, noncovalent interactions, excited states, and transition elements: Two new functionals and systematic testing of four M06-class functionals and 12 other function. *Theor. Chem. Acc.* **2006**, *120*, 215–241. [CrossRef]
27. Zhao, Y.; Schultz, N.E.; Truhlar, D.G. Design of density functionals by combining the method of constraint satisfaction with parametrization for thermochemistry, ther-mochemical kinetics, and noncovalent interactions. *J. Chem. Theory Comput.* **2006**, *2*, 364–382. [CrossRef] [PubMed]
28. Frisch, M.J.; Pople, J.A.; Binkley, J.S. Self-consistent molecular orbital methods 25. Supplementary functions for Gaussian basis sets. *J. Chem. Phys.* **1984**, *80*, 3265–3269. [CrossRef]
29. Dunning, T., Jr.; Hay, P.J. *Modern Theoretical Chemistry*; Schaefer, H., III, Ed.; Plenum: New York, NY, USA, 1977.
30. Soler, J.M.; Artacho, E.; Gale, J.D.; García, A.; Junquera, J.; Ordejón, P.; Sánchez-Portal, D. The SIESTA method for ab initio order-N materials simulation. *J. Phys. Cond. Matt.* **2002**, *14*, 2745–2778. [CrossRef]
31. Perdew, J.P.; Burke, K.; Ernzerhof, M. Generalized Gradient Approximation Made Simple. *Phys. Rev. Lett.* **1996**, *77*, 3865–3868. [CrossRef]
32. Yang, J.; Chen, C. Gemdock: A generic evolutionary method for molecular docking. *Proteins* **2004**, *55*, 288–304. [CrossRef]
33. Thomsen, R.; Christensen, M.H. MolDock: A new technique for high-accuracy molecular docking. *J. Med. Chem.* **2006**, *49*, 3315–3321. [CrossRef]